Journal of Energy and Power Engineering 7 (2013) 2263-2272

Natural Convection of Nanofluid in Cylindrical Enclosure Filled with Porous Media

Manal Hadi Al-Hafidh[1] and Hayder Ibrahim Mohammed[2]

1. Department of Mechanical Engineering, Faculty of Engineering, Baghdad University, Baghdad 964, Iraq

2. Physical Department, Education College, Faculty of Engineering, University of Garmyan, Sulaymaniyah 964, Iraq

Received: March 20, 2013 / Accepted: June 07, 2013 / Published: December 31, 2013.

Abstract: A numerical study has been carried out to investigate the effect of aspect ratio on heat transfer by natural convection of nanofluid taking Cu nano particles and the water as based fluid. The flow is laminar, steady state, axisymmetric two-dimensional in a vertical cylindrical channel filled with porous media. Heat is generated uniformly along the center of the channel with its vertical surface remain with cooled constant wall temperature and insulated horizontal top and bottom surfaces. The governing equations which used are continuity, momentum and energy equations using Darcy law and Boussinesq's approximation which are transformed to dimensionless equations. The finite difference approach is used to obtain all the computational results using the MATLAB-7 program. The parameters affected on the system are Rayleigh number ranging within ($10 \leq Ra \leq 10^3$), aspect ratio ($1 \leq As \leq 5$) and the volume fraction ($0 \leq \varphi \leq 0.2$). The results obtained are presented graphically in the form of streamline and isotherm contour plots and the results show that as φ increase from 0.01 to 0.2 the value of the mean Nusselt number increase 50.4% for Ra = 1,000.

Key words: Laminar natural convection, nanofluid, porous media, vertical cylinder, heat generation.

Nomenclature

Symbols	Description	Units
A	Dimensionless aspect ratio ($A = H/R$)	
C_p	Specific heat at constant pressure	J/kg·K
Da	Darcy number ($Da = K/R^2$)	
g	Acceleration of gravity	m/s^2
H	Axial length of cylinder	m
K	Permeability	m^2
k	Thermal conductivity	W/m·K
k_{nf}	Thermal conductivity of nanofluid	W/m·K
k_{cu}	Thermal conductivity of copper particles	W/m·K
Nu	Local Nusselt number	
Nu_{mean}	Mean Nusselt number	
p	Pressure	N/m^2
T	Temperature	ºC
$\bar{T}$	Dimensionless temperature	
Tc	Cooled temperature for boundary	ºC
R	Radius of the cylinder	m
Ra	Rayleigh number	
r	Radial coordinate	m
$\bar{r}$	Dimensionless radial coordinate	
Vr	Radial velocity component	m/s
$\bar{V}$	velocity vector	
$\bar{v}_r$	Dimensionless radial velocity component	
Vz	Axial velocity component	m/s
$\bar{v}_z$	Dimensionless axial velocity component	
z	Axial coordinate	m
$\bar{z}$	Dimensionless axial coordinate	

Greek Symbols

Symbols	description	Units
α_{nf}	Convective thermal diffusivity of nanofluid	m^2/s
β_{nf}	Volumetric thermal expansion coefficient of nanofluid	1/K
ε	Porosity	
$\boldsymbol{\Psi}$	Dimensionless stream function	
γ	Relaxation factor	
ξ	Represents ψ and $\bar{T}$	
ψ	Stream function	m^2/s
Δ	Difference between two values	
μ_f	Dynamic viscosity of fluid	kg/m·s
μ_{nf}	Dynamic viscosity of nanofluid	kg/m·s
∇	Laplacian in dimensionless cylindrical coordinates	
η	Actual value of the quantity of a point inside	

Corresponding author: Manal Hadi Al-Hafidh, assistant professor, research fields: heat transfer, fluid mechanics and porous media. E-mail: manalhadi2005@yahoo.com.

	the sample volume	
ρ_f	Density of fluid	kg/m^3
ρ_{nf}	Density of nanofluid	kg/m^3
ρ_{cu}	Density of copper particles	kg/m^3
φ	Volume fraction	

1. Introduction

Using nanofluids as a working fluid is an effective approach to meet some challenges associated with the conventional microfluids such as abrasion, clogging, rapid sedimentation and high pressure drop. Furthermore, nanofluids have distinguished thermal features such as high thermal conductivity and high surface to volume ratio, resulting in their perfect thermal performance. That is why nanofluids could be considered a practical approach to alleviate the repercussions of global warming, reduce the carbon footprints in our world, and more importantly, tackle our addiction to fossil fuels. Consequently, nanofluids can be widely used in the heat removal industry; for example, heat removal from electrical circuits. This is why intensive researches focus on the heat transfer augmentation utilizing nanofluids and their potential in cooling industry has been carried out recently in Refs. [1-4].

Nabavitabatabayi [5] investigated the heat transfer performance in an enclosure including nanofluids with a localized heat source. The main objective was to study the influence of several pertinent parameters such as Rayleigh number, solid particle volume fraction of nanoparticles, and the geometry as well as location of the localized heat source on the heat transfer performance of nanofluids.

The results obtained from lattice Boltzmann modeling clearly indicate that heat transfer augmentation is possible using nanofluids in comparison to conventional fluids, resulting in the compactness of many industrial devices.

Heat transfer and fluid flow due to buoyancy forces in a partially heated enclosure using nanofluids is carried out by Ref. [6] using different types of nanoparticles. The flush mounted heater is located to the left of the vertical wall with a finite length. The temperature of the right vertical wall is lower than that of heater while other walls are insulated. The finite volume technique is used to solve the governing equations. Different types of nanoparticles were tested. An increase in mean Nusselt number was found with the volume fraction of nanoparticles for the whole range of Rayleigh number. Heat transfer also increases with increasing of height of heater.

Shahi et al. [7] studied by a numerical method laminar conjugate heat transfer by natural convection and conduction in a vertical annulus formed between an inner heat generating solid circular cylinder and an outer isothermal cylindrical boundary. It is assumed that the two sealed ends of the tube to be adiabatic. The governing equations have been solved using the finite volume approach, using SIMPLE algorithm on the collocated arrangement.

Lin and Violi [8] analyzed the heat transfer and fluid flow of natural convection in a cavity filled with Al/water nanofluid that operates under differentially heated walls. The Navier-Stokes and energy equations are solved numerically, coupling Xu's model for calculating the effective thermal conductivity and Jang's model for determining the effective dynamic viscosity, with the slip mechanism in nanofluids. The heat transfer rates are examined for parameters of non-uniform nanoparticle size, mean nanoparticle diameter, nanoparticle volume fraction, Prandtl number and Grashof number. Decreasing the Prandtl number results in amplifying the effects of nanoparticles due to increased effective thermal diffusivity. The results highlight the range where the heat transfer uncertainties can be affected by the size of the nanoparticles.

Heat transfer enhancement utilizing nanofluids in a trapezoidal enclosure was investigated by Saleh et al. [9] for various pertinent parameters. Transport equations are modeled by a stream-vorticity formulation and solved numerically by finite difference approach. The inclined sloping boundaries are treated by adopting staircase-like zigzag lines. Water-Cu and water-Al nanofluids were tested. The results show that acute sloping wall and Cu nanoparticles with high concentration are effective to enhance the rate of heat transfer.

2. Mathematical Model

The schematic drawing of the geometry and the Cartesian coordinate system employed in solving the problem is shown in Fig. 1.

The mathematical modeling will be set for laminar natural convection heat transfer in a vertical cylinder filled with porous media saturated with nanofluid. The buoyancy effect caused by the density variation produces natural circulation resulting in the fluid motion relative to the bounding solid surface. The buoyancy forces behave as body forces and are included as such in the momentum equation. Under these conditions the continuity, momentum and energy equations are coupled.

2.1 Governing Equations

The effective thermal conductivity of the nano-fluid is approximated by Maxwell-Garnetts model:

$$\frac{k_{nf}}{k_f} = \frac{k_{cu} + 2k_f - 2\phi\ (k_f - k_{cu})}{k_{cu} + 2k_f + \phi\ (k_f - k_{cu})} \tag{1}$$

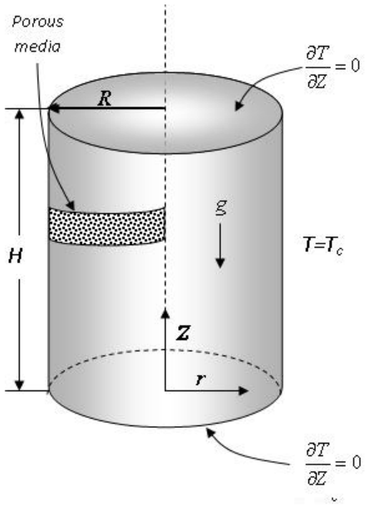

Fig. 1 Geometric configuration, coordinate system and the boundary conditions.

The use of this equation is restricted to spherical nano-particles where it does not account for other shapes of nano-particles. This model is found to be appropriate for studying heat transfer enhancement using nanofluid as in Refs. [7, 10].

The viscosity of the nano-fluid can be approximated as viscosity of a base fluid μ_f containing dilute suspension of fine spherical particles and is given by Ref. [11]:

$$\mu_{nf} = \frac{\mu_f}{(1-\phi)^{2.5}} \tag{2}$$

The effective density of the nanofluid is given as:

$$\rho_{nf} = \phi\ \rho_{cu} + (1-\phi)\ \rho_f \tag{3}$$

The heat capacitance of the nano-fluid is expressed as in Refs. [10, 11]:

$$(\rho \cdot C_p)_{nf} = \phi\ (\rho \cdot C_p)_{cu} + (1-\phi)\ (\rho \cdot C_p)_f \tag{4}$$

The thermo physical properties of water and nanoparticles at 300 K are given in Table 1.

2.1.1 Mass Conservation

$$\frac{1}{r}\frac{\partial (r\,V_r)}{\partial r} + \frac{\partial V_z}{\partial z} = 0 \tag{5}$$

2.1.2 Momentum Equations

The most common model used for flow in the porous media is the Darcy flow model. Darcy's law states that the volume average velocity through the porous material is proportional with the pressure gradient. In three dimensional flows, the Darcy's model as in Ref. [12] is:

(1) Momentum Equation in Axial Direction

$$V_z = -\frac{K}{\mu_{nf}}\left[\frac{\partial p}{\partial z} + \rho_{nf} g\ [1-\beta_{nf}(T - T_c)]\right] \tag{6}$$

(2) Momentum Equation in Radial Direction

Table 1 Thermo physical properties of fluid and nanoparticles.

Physical properties	Cu	Water
C_p (J/kg·K)	385	4,179
ρ (kg/m^3)	8933	997.1
k (W/m·K)	400	0.613
$\alpha \times 10^{-7}$ (m^2/s)	1,163.1	1.47
$\beta \times 10^5$ (1/K)	1.67	21

$$V_r = -\frac{K}{\mu_{nf}}\left[\frac{\partial p}{\partial r}\right] \quad (7)$$

2.1.3 Energy Equation

$$V_r\frac{\partial T}{\partial r}+V_z\frac{\partial T}{\partial z}=\frac{k_{nf}}{(\rho Cp)_{nf}}\left[\frac{1}{r}\frac{\partial}{\partial r}\left(r\frac{\partial T}{\partial r}\right)+\frac{\partial}{\partial z}\left(\frac{\partial T}{\partial z}\right)\right]+\frac{q^{\circ}}{(\rho C_p)_{nf}} \quad (8)$$

2.2 Normalization Parameters

The variables in the governing equations and boundary conditions are transformed to dimensionless formula by employing the following transformation parameters:

$$\bar{r} = \frac{r}{R},\quad \bar{z} = \frac{z}{H},\quad \bar{T} = \frac{T - T_c}{\frac{q^{\circ}\ R^2}{2k_{nf}}},\quad \bar{V}_z = \frac{V_z\ R^2}{H\ \alpha_{nf}}$$

$$\bar{V}_r = \frac{V_r\ R}{\alpha_{nf}},\quad \bar{V}_z = \frac{1}{\bar{r}}\frac{\partial \psi}{\partial \bar{r}},\quad \bar{V}_r = -\frac{1}{\bar{r}}\frac{\partial \psi}{\partial \bar{z}}$$

$$\bar{P} = \frac{p\ K\ R^2}{\alpha_{nf}\ \mu_{nf}\ H^2} = \frac{p\ K\ A}{\alpha_{nf}\ \mu_{nf}},\quad Da = \frac{K}{R^2},$$

$$Ra = \frac{g(\rho\beta)_f\ K\ q\ D^2}{2\ k_f\ \mu_f\ \alpha_f} \quad (9)$$

By using the relation above Eqs. (6)-(8) become:

2.2.1 Momentum Equation

$$A^2 = \left(\frac{1}{\hat{R}}\frac{\partial^2 \Psi}{\partial \hat{R}^2} - \frac{1}{\hat{R}^2}\frac{\partial \Psi}{\partial \hat{R}}\right) + \frac{1}{\hat{R}}\frac{\partial^2 \Psi}{\partial \hat{Z}^2} = Ra * A * C_1\left[\frac{\partial \bar{T}}{\partial \bar{r}}\right] \quad (10)$$

where:

$$C_1 = \frac{(1-\varphi)^{2.5}}{\alpha_f}\left[(1-\varphi) + \varphi\frac{(\rho\beta)_{cu}}{(\rho\beta)_f}\right] \quad (11)$$

2.2.2 Energy Equation

$$\frac{1}{\hat{R}}\frac{\partial \Psi}{\partial \hat{R}}\frac{\partial \bar{T}}{\partial \hat{Z}} - \frac{1}{\hat{R}}\frac{\partial \bar{T}}{\partial \hat{R}}\frac{\partial \Psi}{\partial \hat{Z}} = \varphi\left(\frac{1}{\hat{R}}\frac{\partial}{\partial \hat{R}}\left(\hat{R}\frac{\partial \bar{T}}{\partial \hat{R}}\right) + \frac{1}{A^2}\frac{\partial^2 \bar{T}}{\partial \hat{Z}^2}\right) + 2 \quad (12)$$

And the boundary condition will be:

$$\left.\begin{aligned} &\bar{r} = 0,\ \psi = 0,\ \frac{\partial \bar{T}}{\partial \bar{r}} = 0 \\ &\bar{r} = 1,\ \psi = 0,\ \bar{T} = 0 \\ &\bar{z} = 0,\ \psi = 0,\ \frac{\partial \bar{T}}{\partial \bar{z}} = 0 \\ &\bar{z} = 1,\ \psi = 0,\ \frac{\partial \bar{T}}{\partial \bar{z}} = 0 \end{aligned}\right\} \quad (13)$$

2.3 Calculation of Local and Mean Nusselt Number

The local Nusselt number at the wall is defined as:

$$Nu = -\left(\frac{k_{nf}}{k_f}\right)\left(\frac{d\bar{T}}{d\bar{r}}\right) \qquad at\ \bar{r} = 1 \quad (14)$$

The mean Nusselt number along the wall can be expressed as:

$$Nu_{mean} = \int_0^1 Nu\ dz \quad \text{where } d\bar{T} = d\theta \quad (15)$$

3. Numerical Solution

The new algebra equations system can be solved using some of known techniques, like relaxation method, to give approximate values of the dependent variables at a number of discrete points called (grid points or nodes) in the computational domain. A grid was established by subdividing the computational domain in the *R* and *Z* directions with indexes *i* and *j* that are integers describing the number of radial grid lines from the center of the cylinder and the number of axial grid lines from the lower to upper surface respectively. The spacing of the grid lines in the R-direction is uniform and given by (Δr) and that of the grid lines in the Z-direction is also uniform and given by (Δz). The number of the grid points will be ($m \times n$) where (m) represents the number of gridlines in the R-direction and equals $[(1/\Delta\bar{r}) + 1]$ while (n) represents the number of gridlines in the Z-direction and equals $[(1/\Delta\bar{z}) + 1]$.

The partial differential Eqs. (9) and (10) were finite-differenced using central difference schemes for all of the derivatives. In particular, let ξ represents ψ and $\overline{T}$ then:

$$\left.\begin{aligned}
&\Delta\bar{r} = \Delta\bar{z}\ ,\ \Delta\bar{r}_i = \Delta\bar{r}_{i+1}\ ,\ \Delta\bar{z}_j = \Delta\bar{z}_{j+1}\\
&\frac{\partial\xi}{\partial\bar{r}} = \frac{\xi_{(i+1,j)} - \xi_{(i-1,j)}}{2\Delta\bar{r}}\\
&\frac{\partial\xi}{\partial\bar{z}} = \frac{\xi_{(i,j+1)} - \xi_{(i,j-1)}}{2\Delta\bar{z}}\\
&\frac{\partial^2\xi}{\partial\bar{r}^2} = \frac{\xi_{(i+1,j)} - 2\xi_{(i,j)} + \xi_{(i-1,j)}}{\Delta\bar{r}^2}\\
&\frac{\partial^2\xi}{\partial\bar{z}^2} = \frac{\xi_{(i,j+1)} - 2\xi_{(i,j)} + \xi_{(i,j-1)}}{\Delta\bar{z}^2}
\end{aligned}\right\} \tag{16}$$

In terms of the above expressions momentum and energy equations become:

3.1 Momentum Equation

$$\frac{A^2}{\bar{r}_{(i)}}\frac{\Psi_{(i+1,j)} - 2\Psi_{(i,j)} + \Psi_{(i-1,j)}}{\Delta\bar{r}^2} - \frac{A^2}{\bar{r}_{(i)}^2}\frac{\Psi_{(i+1,j)} - \Psi_{(i-1,j)}}{2\Delta\bar{r}} + \frac{\Psi_{(i,j+1)} - 2\Psi_{(i,j)} + \Psi_{(i,j-1)}}{\bar{r}_{(i)}\Delta\bar{z}^2} = Ra\,A\,C_1\frac{\overline{T}_{(I+1,J)} - \overline{T}_{(I-1,J)}}{2\Delta\bar{r}} \tag{17}$$

3.2 Energy Equation

$$\frac{1}{\bar{r}_{(i)}}\frac{\Psi_{(i+1,j)} - \Psi_{(i-1,j)}}{2\,\Delta\bar{r}} * \frac{\overline{T}_{(i,j+1)} - \overline{T}_{(i,j-1)}}{2\Delta\bar{z}} - \frac{1}{\bar{r}_{(i)}}\frac{\overline{T}_{(I+1,J)} - \overline{T}_{(I-1,J)}}{2\,\Delta\bar{r}} * \frac{\Psi_{(i,j+1)} - \Psi_{(i,j-1)}}{2\,\Delta\bar{z}^2} = \varphi\left[\frac{\overline{T}_{(I+1,J)} - 2\overline{T}_{(I,J)} + \overline{T}_{(I-1,J)}}{\Delta\bar{r}^2} + \frac{1}{\bar{r}_{(i)}}\frac{\overline{T}_{(I+1,J)} - \overline{T}_{(I-1,J)}}{2\Delta\bar{r}}\right] + \frac{\varphi}{A^2}\frac{\overline{T}_{(i,j+1J)} - 2\overline{T}_{(i,j)} + \overline{T}_{(I,J-1)}}{\Delta\bar{z}^2} + 2 \tag{18}$$

4. Relaxation Method

As a solution method for the system of algebraic Eqs. (17) and (18) obtained from the discretization of governing differential equations, iterative relaxation method was used. In relaxation methods, the value of the variable to be used for obtaining the solution in the next iteration is the value in the current iteration plus a fraction of the difference between the current value and the predicted value as in Ref. [13]:

$$\phi_p^{\zeta+1} = \phi_p^{\zeta} + \gamma\left(\frac{\sum\left(a_{\zeta b} * \phi_{\zeta b}\right) + b}{a_p} - \phi_p^{\zeta}\right) \tag{19}$$

where:

$\gamma > 0$ is the relaxation factor;

$\phi_p^{\zeta+1}$ is the value of the state variable at node P to be used for the next iteration;

ϕ_p^{ζ} is the value of the state variable at node P form current iteration;

$\phi_{\zeta b}$ is the values of the variable at the surrounding nodes and $a_{\zeta b}$ and b are the constants from the discretized equation.

Relaxation method is a relatively simple method and can be easily altered when changing the grid structure or parameters affecting convergence but, the major disadvantage is the task of choosing the optimum relaxation coefficient (γ) for a given situation. The grid that used in this work was (41 × 61) and shown in Fig. 2. Generally, the temperature is over relaxed and/or the stream function is under relaxation.

5. Results and Discussion

Finite difference solution for laminar natural convection flow of a water based nanofluids in a vertical enclosure filled with porous media was presented for half the cylinder due to the symmetry exist.

In Fig. 3 for (φ = 0.2 and 0.01, Ra^* = 10 and A = 5 where $A = H/R$), it is clear that the temperature ranged (0.0083-0.00075) from the hotter region to the cold one for φ = 0.2 and (0.048-0.0043) for φ = 0.01, that is the temperature decrease as φ increase this means that the heat transfer enhance as φ increase. The streamlines ranged (0.0226-0.2496) for φ = 0.2 and ranged (0.04-0.4408) for φ = 0.01, this is due to the increase in heat transfer as φ increase which cause the region to be cooled and so the values of the stream decrease.

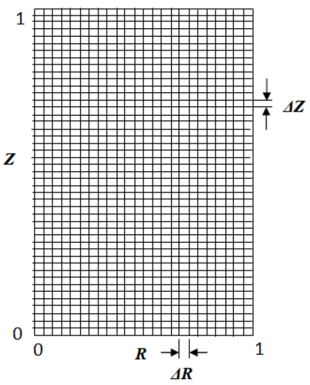

Fig. 2 Domain discretization in a cylindrical enclosure at *A* = 1.

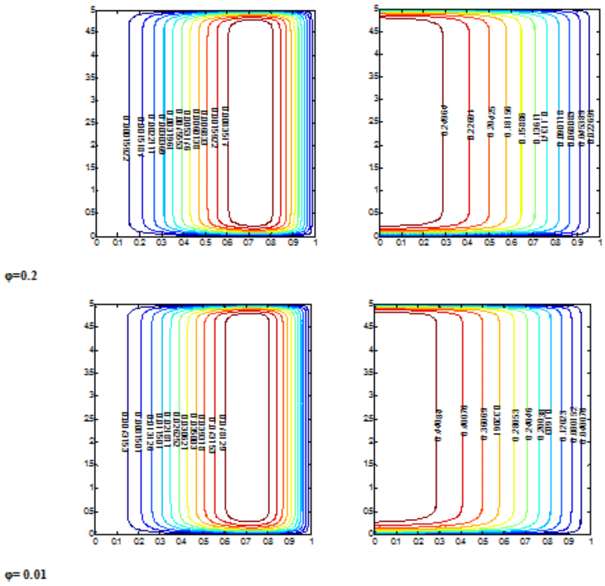

Fig. 3 Streamlines and isotherms contours for *Ra* = 10, *A* = 5.

The comparison between Figs. 3 and 4 show that for Ra^* = 10, as aspect ratio decrease to A = 1 or in other word R increase the temperature decrease and the values of streamlines decrease and the convection heat transfer will be the dominant mode.

When Ra^* increase to 1,000 for the same aspect ratio A = 1, as shown in Fig. 5, it is clear that a little decrease in temperature appear, this behavior was happened because the increasing of the *Ra* cause an increasing in the velocity and more circulation between the layers of the fluid that caused the temperature to be dropped.

Figs. 6 and 7 show the effect of *Ra*, *A* and φ on the temperature distribution at the centerline along the cylinder length. Fig. 6 shows the variation of temperature along the cylinder centerline with increasing

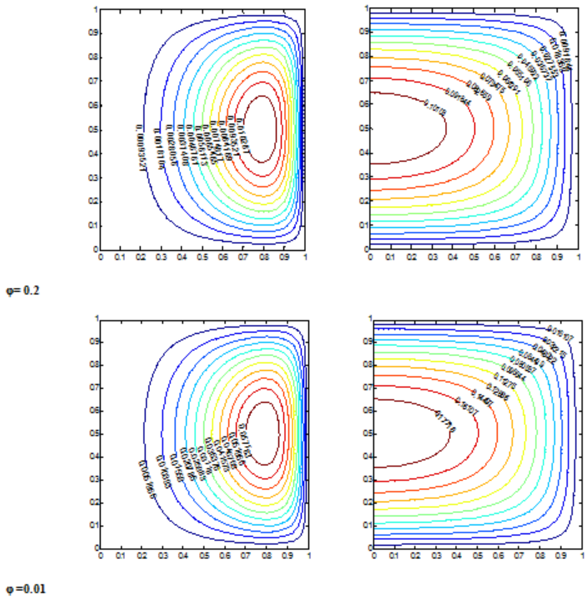

Fig. 4 Streamlines and isotherms contours for *Ra* = 10, *A* = 1.

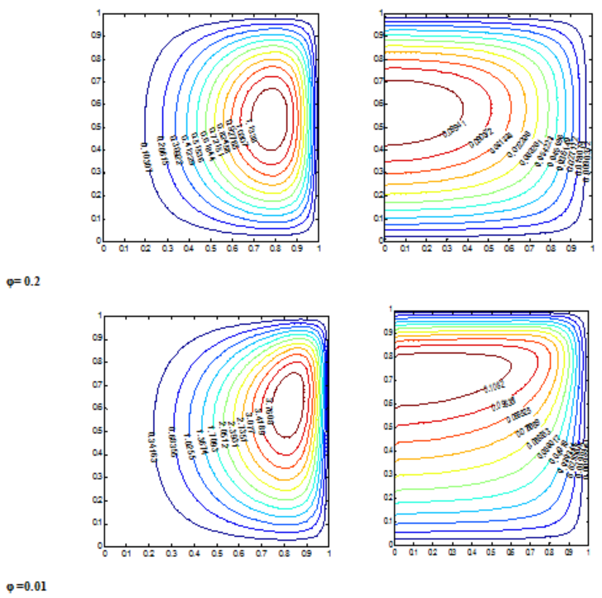

Fig. 5 Streamlines and isotherms contours for *Ra* = 1,000, *A* = 1.

of the volume fraction. This figure illustrate that the effect of φ is very significant and the temperature distribution is symmetric where the maximum temperature appear in the middle of the cylinder and that the decrease in maximum temperature as φ increase from 0.05 to 0.2 for *Ra* = 10 is 55% while for *Ra* = 1,000 it is 35.38%.

Fig. 7 shows that for aspect ratio A = 5 or in other words for narrow region even for high values of *Ra* the temperature values will be increased due to the decrease

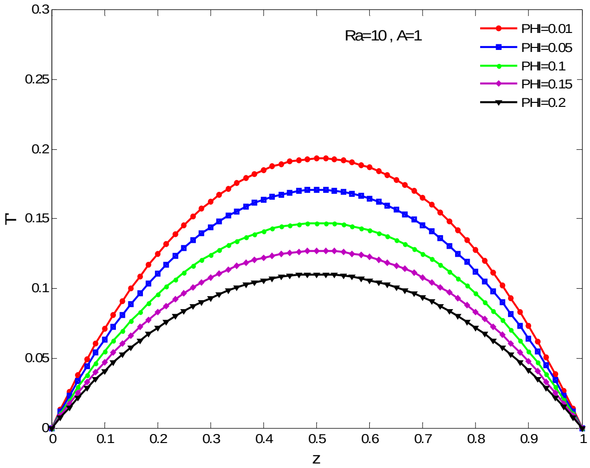

Fig. 6 Variation of temperature in center line along the cylinder length for *Ra* = 1,000, *A* = 1 and different *φ*.

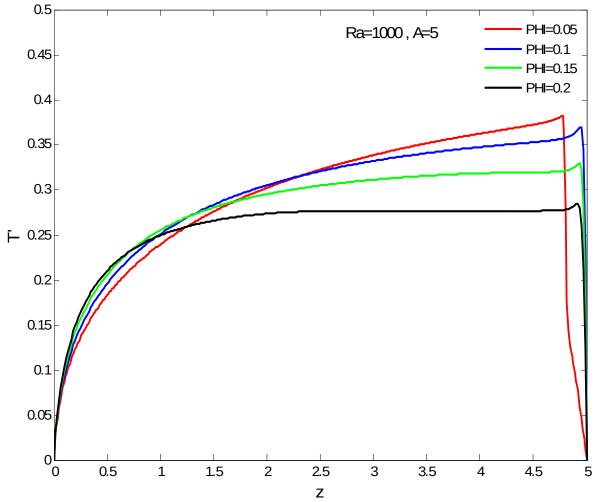

Fig. 7 Variation of temperature in center line along the cylinder length for *Ra* = 100, *A* = 5 and different *φ*.

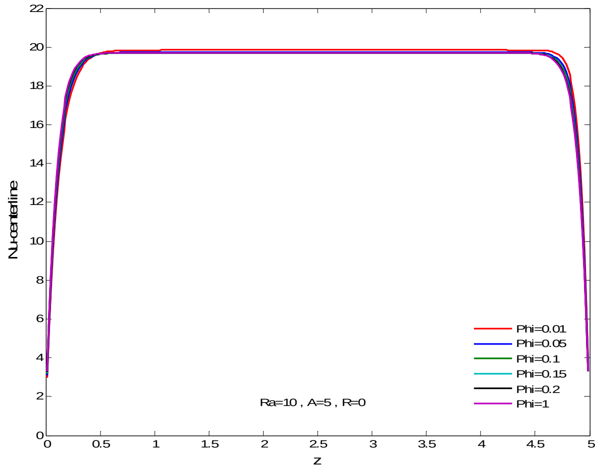

Fig. 8 Variation of local *Nu* in center line along the cylinder length for *Ra* = 10, *A* = 5 and different *φ*.

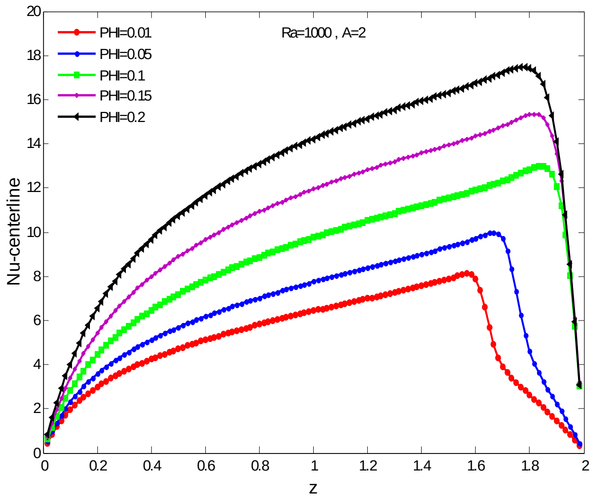

Fig. 9 Variation of local *Nu* in center line along the cylinder length for *Ra* = 1,000, *A* = 2 and different *φ*.

in heat transfer and the effect of adding nanoparticles is very significant. As *φ* increase, the temperature decrease where it have a higher values at the upper portion of the cylinder because heat diffusion in the system decrease causing the temperature to be increased and the fluid moved and collected near the upper surface.

Figs. 8 and 9 show the effect of *Ra*, *A* and *φ* on local *Nu* at the centerline. Fig. 8 shows the variation of local *Nu* along the cylinder centerline with increasing of the volume fraction. This figure illustrates that for *A* = 5 and low values of *Ra* (which means cooled region) the effect of *φ* is insignificant and local *Nu* values are symmetric in the upper and lower portions of the cylinder.

Fig. 9 shows that as *Ra* increase and aspect ratio decrease in other word for hot regions the effect of adding nanoparticles is very significant and that as *φ* increase local *Nu* increase and have a high values at the upper portion of the cylinder because heat diffusion in the system increase with increasing of *φ* and the fluid will moved and collected near the upper surface.

Fig. 10 illustrates the variation of local *Nu* in the radial direction where it is clear that the values of local *Nu* are almost constant from the centerline toward the cylinder wall. As *r* is nearly equal 0.6, the values will be decreased and for narrow cylinders (*A* = 5), the local *Nu* increase as shown in Fig. 11.

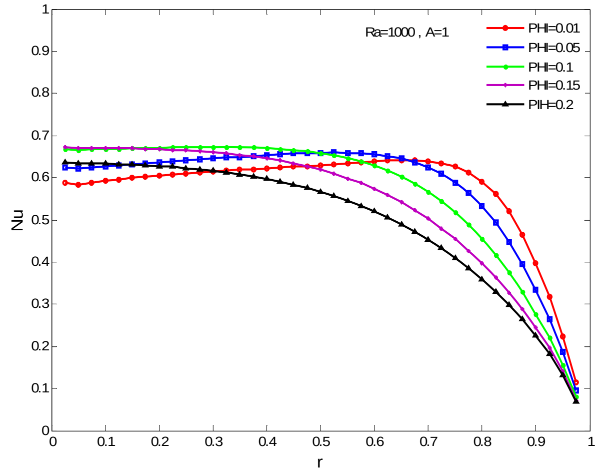

Fig. 10 Variation of local *Nu* in center line along the cylinder radius for *Ra* = 1,000, *A* = 1 and different *φ*.

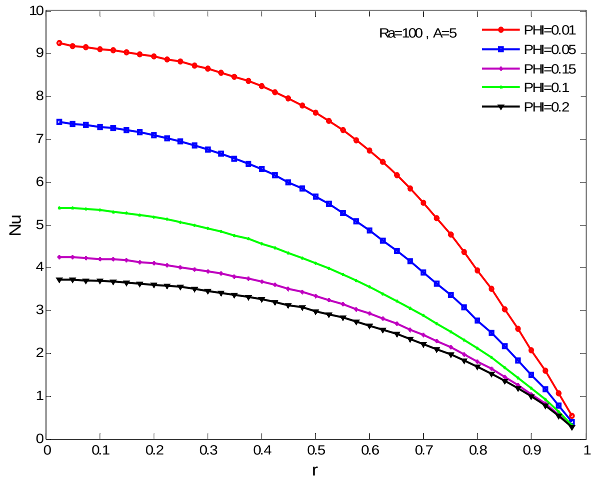

Fig. 11 Variation of local *Nu* in center line along the cylinder radius for *Ra* = 100, *A* = 5 and different *φ*.

Fig. 12 illustrates the variation of Nu_{mean} with Ra at A = 1 for different values of φ, it is clear that the value of Nu_{mean} increase with Ra and significantly effect of φ appear where as φ increase from 0.01 to 0.2 the value of the mean Nusselt number increase 50.4% for Ra = 1,000.

Fig. 13 shows the variation of Nu_{mean} with Ra for φ = 0.1 and different values of A. It is clear that the value of Nu_{mean} was increased with the increasing of Ra and that the value of Nu_{mean} decrease as A decrease because the region will be wide and cooled so the heat transfer increase.

The variation of Nu_{mean} with φ is illustrated in Fig. 14 for A = 1 and different Ra, it is clear that for high

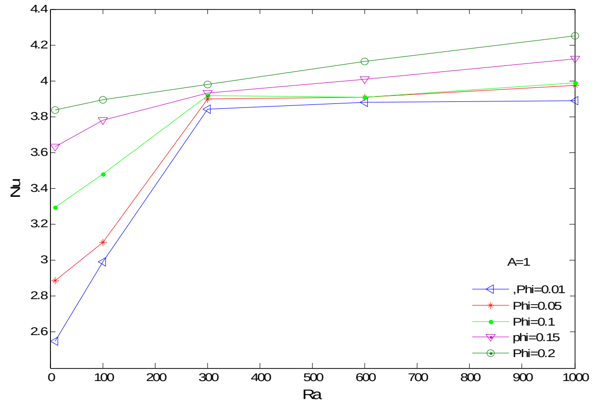

Fig. 12 Variation of *Nu* with *Ra* for *A* = 1 and different *φ*.

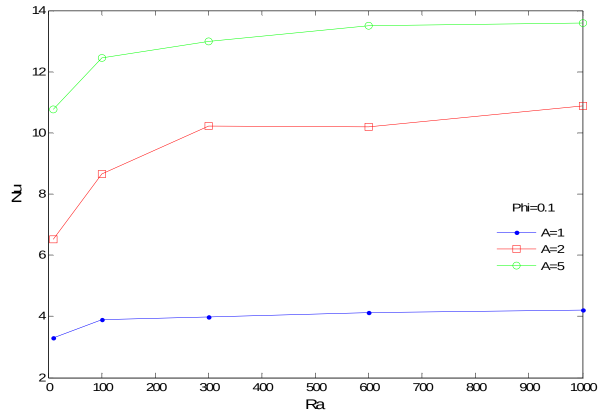

Fig. 13 Variation of *Nu* with *Ra* for *φ* = 0.1 and different *A*.

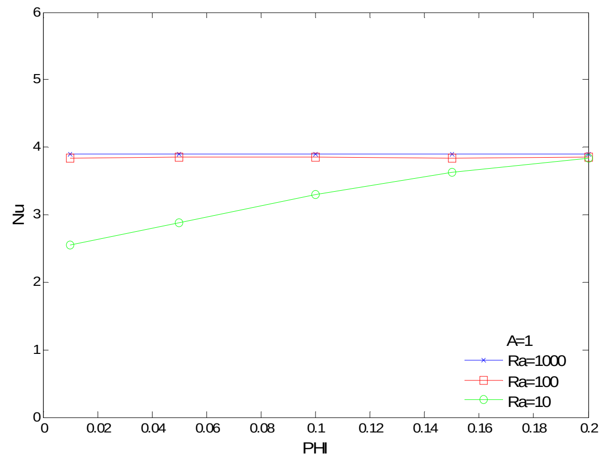

Fig. 14 Variation of *Nu* with *φ* for *A* = 1 and different *Ra*.

values of Ra, the values of Nu_{mean} are almost constant while for Ra = 10, adding nanoparticles caused significant increase in Nu_{mean}.

Fig. 15 shows the variation of Nu_{mean} with φ for Ra = 100 and different values of A, where it is clear that Nu_{mean} almost constant and increased as A increase.

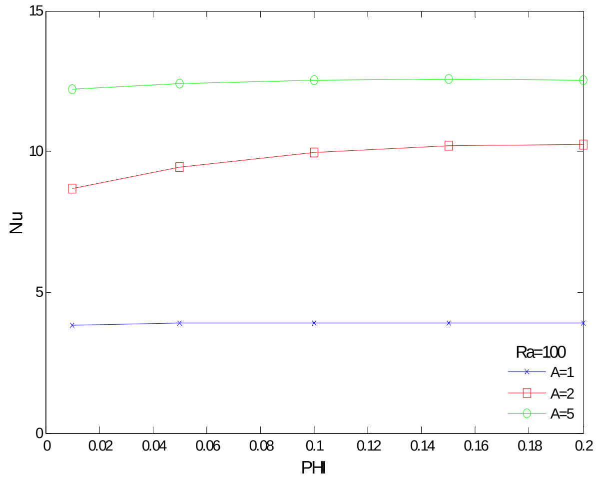

Fig. 15 Variation of *Nu* with *φ* for *Ra* = 100 and different *A*.

6. Conclusions

The following major conclusions can be drawn from the study:

(1) The temperature decrease as φ increase this means that the heat transfer enhance as φ increase. As aspect ratio decrease to $A = 1$ or in other word R increase the temperature decrease and the values of streamlines decrease and the convection heat transfer will be the dominant mode.

(2) The effect of φ is very significant and the temperature distribution is symmetric where the maximum temperature appear in the middle of the cylinder and that the decrease in maximum temperature as φ increase from 0.05 to 0.2 for $Ra = 10$ is 55% while for $Ra = 1{,}000$ it is 35.38%.

(3) As Ra increase and aspect ratio decrease in other word for hot regions the effect of adding nanoparticles is very significant and that as φ increase local Nu increase and have a high values at the upper portion of the cylinder.

(4) The values of local Nu are almost constant from the centerline toward the cylinder wall and as r is nearly equal 0.6 the values will be decreased.

(5) Nu_{mean} increase with Ra and significantly effect of φ appear where as φ increase from 0.01 to 0.2 the value of the mean Nusselt number increase 50.4% for $Ra = 1{,}000$.

(6) Nu_{mean} was increased with the increasing of Ra and that the value of Nu_{mean} decrease as A decrease.

(7) For high values of Ra, the values of Nu_{mean} are almost constant while for $Ra = 10$, adding nanoparticles caused significant increase in Nu_{mean}.

References

[1] K. Khanafer, K. Vafai, M. Lightstone, Buoyancy driven heat transfer enhancement in a two-dimensional enclosure utilizing nanofluids, Int. J. Heat Mass Transfer 46 (19) (2003) 3639-3653.

[2] S.M. Aminossadati, B. Ghasemi, Natural convection cooling of a localized heat source at the bottom of a nanofluid-filled enclosure, Eur. J. Mech. B. Fluids 28 (5) (2009) 630-640.

[3] H.F. Oztop, E. Abu-Nada, Numerical study of natural convection in partially heated rectangular enclosures filled with nanofluids, Int. J. Heat Fluid Flow 29 (5) (2008) 1326-1336.

[4] D. Wen, Y. Ding, Formulation of nanofluids for natural convective heat transfer applications, Int. J. Heat Fluid Flow 26 (6) (2005) 855-864.

[5] M. Nabavitabatabayi, E. Shirani, M.H. Rahimian, Investigation of heat transfer enhancement in an enclosure filled with nanofluids using multiple relaxation time lattice Boltzmann modeling, Int. communication of Heat and Mass Transfer 38 (2011) 128-138.

[6] H.F. Oztop, E. Abu-Nada, Numerical study of natural convection in partially heated rectangular enclosures filled with nanofluids, International Journal of Heat and Fluid Flow 29 (5) (2008) 1326-1336.

[7] M. Shahi, A.H. Mahmoudi, F. Talebi, A numerical investigation of conjugated-natural convection heat transfer enhancement of a nanofluid in an annular tube driven by inner heat generating solid cylinder, Int. communication of Heat and Mass Transfer 38 (4) (2011) 533-542 .

[8] K.C. Lin, A. Violi, Natural convection heat transfer of nanofluids in a vertical cavity: Effects of nonuniform particle diameter and temperature on thermal conductivity, International Journal of Heat and Fluid Flow 31 (2010) 236-245.

[9] H. Saleh, R. Roslan, I. Hashim, Natural convection heat transfer in a nanofluid filled trapezoidal enclosure, Int. of Heat and Mass Transfer 54 (2011) 194-201.

[10] R. Nazar, L. Tham, I. Pop, D.B. Ingham, Mixed convection boundary layer flow from a horizontal circular cylinder embedded in a porous medium filled with a nanofluid, Transp. Porous Med. 86 (2) (2011) 517-536.

[11] M. Esmaeilpour, M. Abdollahzadeh, Free convection and entropy generation of nanofluid inside an enclosure with different patterns of vertical wavy walls, International

Journal of Thermal Science 52 (2012) 127-136.

[12] B.X. Wang, X. Zhang, Natural convection in liquid saturated porous media between concentric inclined cylinders, Int. J. Heat and Mass Transfer 33 (5) (1990) 827-833.

[13] N. Massarotti, P. Nithiarasu, A. Carotenuto, Microscopic and macroscopic approach for natural convection in enclosures filled with fluid saturated porous medium, Int. J. of Numerical Methods for Heat and Fluid Flow 13 (7) (2003) 862-886.